Radiology Case Reports 16 (2021) 3721–3728

Available online at www.sciencedirect.com

ScienceDirect

journal homepage: www.elsevier.com/locate/radcr

Case report

Carotid computed tomography angiography after cobalt-based alloy carotid artery stenting using ultra-high-resolution computed tomography with model-based iterative reconstruction ☆,☆☆

Shingo Kayano, RT, PhD[a,*], *Hideki Ota, MD, PhD*[b], *Yoshimichi Sato, MD*[c], *Toshiki Endo, MD, PhD*[c,d], *Kuniyasu Niizuma, MD, PhD*[c,d,e], *Ichiro Suzuki, MD, PhD*[f], *Tsuyoshi Kawamura, MD, PhD*[f], *Kei Takase, MD, PhD*[b]

[a] *Department of Radiological Technology, Tohoku University Hospital, 1 1 Seiryo machi, Aoba ku, Sendai, Miyagi 980-8574, Japan*
[b] *Department of Diagnostic Radiology, Tohoku University Graduate School of Medicine, Sendai, Japan*
[c] *Department of Neurosurgery, Tohoku University Graduate School of Medicine, Sendai, Japan*
[d] *Department of Neurosurgical Engineering and Translational Neuroscience, Tohoku University Graduate School of Medicine, Sendai, Japan*
[e] *Department of Neurosurgical Engineering and Translational Neuroscience, Graduate School of Biomedical Engineering, Tohoku University, Sendai, Japan*
[f] *Department of Neurosurgery, Hachinohe City Hospital, Hachinohe, Japan*

ARTICLE INFO

Article history:
Received 26 August 2021
Revised 31 August 2021
Accepted 4 September 2021

ABSTRACT

In conventional carotid computed tomographic angiography, the artifacts of the stent vary depending on the structure and characteristics of the alloy type. Cobalt-based alloy stents have been reported to exhibit high artifacts, and accurate evaluation of the internal lumen can be difficult. Recently, ultra-high-resolution computed tomography scanner systems have become available for clinical practice. The primary features of this computed tomography scanner are a 0.25-mm detector row width and a 1024 × 1024 matrix. We report a case-series of carotid artery stenting using a cobalt-based alloy stent scanned by an

☆ Acknowledgments: The authors thank 2 radiological technologists; Hitoshi Nemoto, R.T., M.S. and Kazuki Shimada, R.T., M.S. for their excellent help in the 3D reconstruction images, and would like to thank Editage (www.editage.com) for English language editing. This research did not receive any specific grant from funding agencies in the public, commercial, or not-for-profit sectors.
☆☆ Competing interests: Hideki Ota and Kei Takase were supported by research grant from Canon Medical Systems, and the other authors report no conflicts of interest.
* Corresponding author. S. Kayano.
E-mail address: s_kayano@med.tohoku.ac.jp (S. Kayano).
https://doi.org/10.1016/j.radcr.2021.09.003

Keywords:
Carotid artery stenting
Cobalt-based alloy stents
Computed tomography angiography
Ultra-high-resolution computed tomography
Model-based iterative reconstruction

ultra-high-resolution computed tomography scanner system and model-based iterative reconstruction. We also report that the combination of the ultra-high-resolution computed tomography scanner system with model-based iterative reconstruction would be useful to evaluate vessel patency after placement of a cobalt-based alloy stent.

Introduction

Carotid artery stenting (CAS) is an alternative treatment for carotid endarterectomy for high-risk patients with carotid artery stenosis; its safety and effectiveness are being recognized worldwide [1–4]. However, a potential drawback of CAS includes restenosis within 2 years after CAS in 4%-8% of patients [5,6].

Ultrasound and computed tomographic angiography (CTA) are non-invasive imaging modalities used to evaluate the development of neointimal formations in patients after CAS [5–9]. The advantages of CTA include visualization of the entire carotid artery and its non-operator-dependent method [10]. Furthermore, it can provide a high-quality image of the internal lumen of a stent and demonstrate restenosis [8,9,11]. However, the artifacts of the stent in conventional carotid CTA vary, depending on the structure and characteristics of the alloy type; this can further limit accurate evaluation [12]. In particular, cobalt-based alloy stents have been reported to show strong artifacts on CTA [13]. Information on the stent type is the most important consideration in choosing an appropriate imaging modality and technique for follow-up in non-invasive examinations [12,14,15].

Recently, an ultra-high-resolution CT (UHRCT) scanner system (Aquilion Precision, Canon Medical Systems, Otawara, Japan) became available in clinical practice. The UHRCT scanner system has a smaller detector element and focal spot as compared with conventional CT systems; it allows acquisition of images with higher spatial resolution in both in-plane and z-axis directions [16]. In particular, the primary features of the UHRCT scanner are a 0.25-mm detector row width and a 1024×1024 matrix. However, the UHRCT scanner system has a high image noise [17] because of the relatively short number of photons per detector. To address this disadvantage, an iterative reconstruction (IR) algorithm is implemented in the UHRCT scanner system. A model-based IR (MBIR) algorithm has been reported to be superior in reducing image noise and improving the image quality and spatial resolution over a conventional filtered back projection (FBP) and hybrid-type IR [18–20]. These technical innovations allow detailed vascular assessment with carotid artery stents.

We have experienced some cases of carotid CTA after CAS using a cobalt-based alloy stent assessed with a UHRCT scanner system. The walls of the stents were assessed better as compared with conventional CTA. We report a case series of CAS using a cobalt-based alloy stent assessed by a UHRCT scanner system with MBIR. Case details are summarized in Table 1.

Case series

Case 1

A 46-year-old-man with acute left carotid artery occlusion due to dissection of the left carotid artery underwent Carotid Wallstent Monorail, (CWS; Boston Scientific, Natick, MA, USA) placement and thrombectomy. Two months after CAS, CTA was performed to evaluate in-stent restenosis and vessel patency.

The strut structure of the stent is clearly illustrated in volume rendering image (Fig. 1A). The MBIR image shows further dramatic improvement of artifacts from healing teeth, and image noise reduction than the FBP image (Figs. 1B and C).

Case 2

A 76-year-old symptomatic man with high-grade right carotid artery stenosis underwent CWS placement in our institution. After 2 years, in-stent restenosis was suspected, and CTA was performed using a UHRCT scanner system.

Curved planar reformation (CPR) image using MBIR reconstruction method indicated in-stent restenosis and intimal formation (Fig. 2A). Digital subtraction angiography revealed in-stent restenosis and intimal formation (Fig. 2B). The DSA image supports the validity of this CPR image.

Case 3

A 79-year-old symptomatic man with high-grade left carotid artery stenosis underwent CWS placement in our institution. The patient underwent CTA and carotid ultrasonography 1 week, 3 months, and 6 months after CAS.

The changes in intimal formations over time are clearly shown (white arrowheads) in CPR images (Fig. 3A, 3B, and 3C). In the ultrasonography images, black arrows indicate CWS, white arrowheads indicate time-dependent intimal formations (Figs. 3D, E, and F). Cross-sectional images show the development of intimal formations over time (Figs. 3G, H, and I).

Control case

A 77-year-old symptomatic man with high-grade left carotid artery stenosis underwent CWS placement in our institution. A follow-up carotid CTA study using a conventional CT scanner system (Aquilion ONE ViSION Edition; Canon Medical Systems, Otawara, Japan) was performed 1 month after CAS (Figs. 4A and B).

Table 1 – Case details.

Parameter	Case 1	Case 2	Case 3	Control case
Age (y)	46	76	79	77
Sex	Male	Male	Male	Male
Condition of patient	Occlusion due to dissection	Stenosis with symptomatic	Stenosis with symptomatic	Stenosis with symptomatic
Stent	CWS (10 × 31 mm)	CWS (10 × 31 mm)	CWS (10 × 31 mm)	CWS (10 × 31 mm)
CT machine	Aquilion Precision	Aquilion Precision	Aquilion Precision	Aquilion ONE ViSION Edition
Tube voltage (kVp)	100	100	100	100
Tube current	AEC: SD 9 @ 0.5 mm	AEC: SD 9 @ 0.5 mm	AEC: SD 9 @ 0.5 mm	AEC: SD 11 @ 0.5 mm
Reconstruction method	FBP MBIR	MBIR	MBIR	Hybrid IR
Kernel	FC 15 FIRST	FIRST	FIRST	FC 21
Iterative level	– STND	STND	STND	AIDR 3D eMild
Thickness (mm)	0.25	0.25	0.25	0.5
Display field of view size (mm)	240	240	240	240
Matrix	1024	1024	1024	512
$CTDI_{vol}$ (mGy)	9.6	9.6	9.6	15.1
DLP (mGy.cm)	338.0	357.2	337.9 ± 16.7	561.4
Injector	Dual Shot GX 7	Dual Shot GX 7	Dual Shot GX 7	Dual Shot GX 7
Contrast medium	iomeprol 300	iomeprol 300	iomeprol 300	iohexol 350
Injection rate (mL/s)	4.9	5.1	4.8	3.9
Injection volume (mL)	59	62	58	46
Saline flash (mL)	25	25	25	25

CWS, Carotid Wallstent Monorail; AEC, auto exposure control; FBP, filtered back projection; MBIR, model based iterative reconstruction; FIRST, forward projected model-based iterative reconstruction solution; AIDR, adaptive iterative dose reduction.

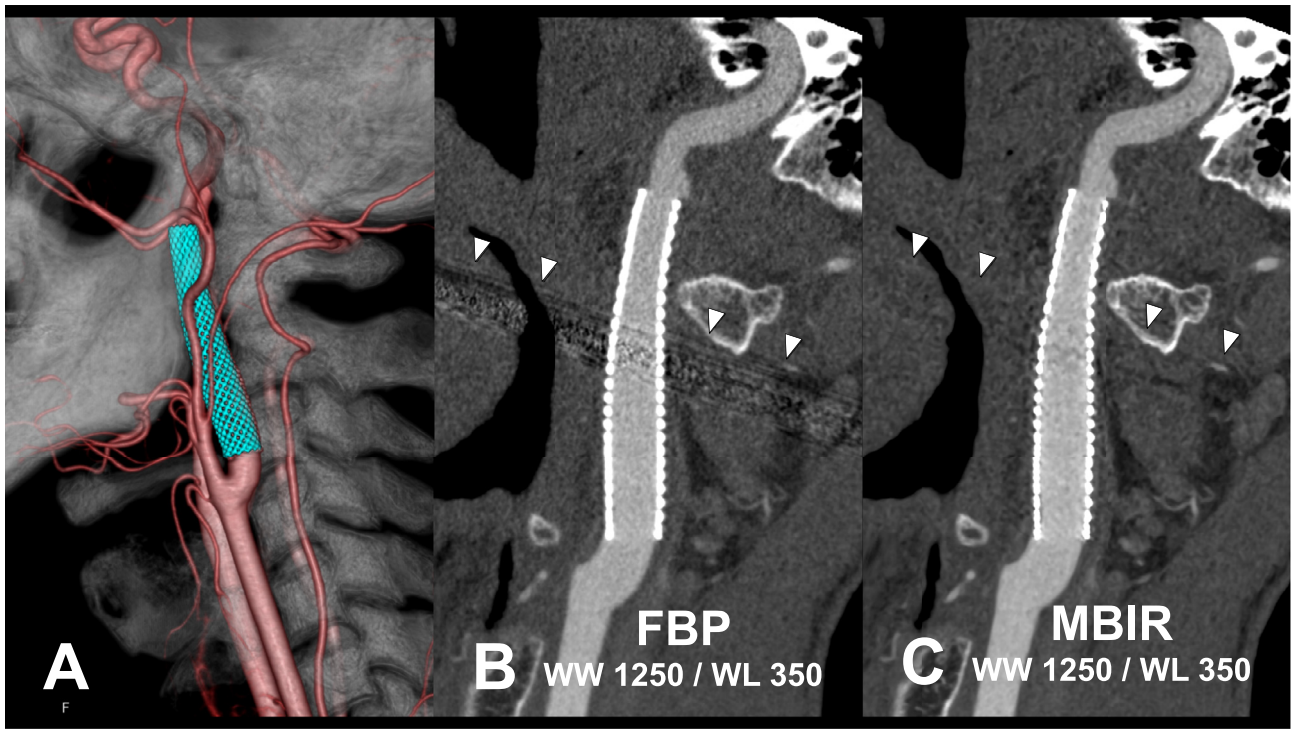

Fig. 1 – A 46-year-old-man. (A) Volume rendering images, (B) and (C) Curved planar reformation images with filtered back projection (FBP) and model-based iterative reconstruction (MBIR), respectively. The MBIR image shows further dramatic improvement of artifacts from healing teeth (white arrowheads), and image noise reduction than the FBP image.

Discussion

To the best of our knowledge, this is the first report of CAS using a cobalt-based alloy stent assessed by the UHRCT scanner system and MBIR. The combination of the UHRCT scanner system and MBIR suggests dramatic improvement of artifacts from stents and treated teeth. It could obtain an image quality of CTA that could be improved after CAS and allow detailed evaluation of vessel patency after CAS. We expect that these innovative technologies will avoid an invasive DSA examination and consequently contribute to reducing healthcare costs.

CWS wires are manufactured from a biomedical grade cobalt-chromium-iron-nickel-molybdenum alloy containing an enhanced radiopaque tantalum core [21]. The x-ray energy and the linear attenuation coefficient of the material need to be considered to reduce artifacts in CT images. In particular, the linear attenuation coefficient increases with the atomic number of a substance. The atomic numbers of each substance in the wires of the CWS are cobalt: 27, chromium: 24, iron: 26, nickel: 28, molybdenum: 42, and tantalum used for x-ray visibility was 73. Sakai *et al.* reported that CWS showed more severe artificial narrowing [13], and Köhler *et al.* who evaluated peripheral stents, reported that tantalum stents showed poor in-stent visibility because of blooming artifacts [22]. These reports indicate that tantalum causes severe artificial narrowing. A similar artifact, shown in Figure 4B, is seen in the control case scanned with a conventional CT scanner system. In contrast, the cases scanned by the UHRCT scanner system shows a thinner depiction of stent strut structures and no severe artificial narrowing because of artifacts from the stent. Onishi *et al.* who compared the conventional CT and UHRCT scanner system for evaluating renal artery stent with phantom models, reported that the metal artifacts of the UHRCT scanner system were significantly less than those of the conventional CT [16]. Similar to their report, the image quality of the carotid CTA using the UHRCT scanner system was significantly better than the image quality of the conventional CT scanner system because of the high spatial resolution and the reduction in metal artifacts from the stents.

The matrix size and slice thickness in conventional CT have been 512 × 512 and 0.5-0.625 mm respectively. The UHRCT scanner system is different in the detector element size and the focal spot size than conventional CT systems, producing images with a matrix of 1024 × 1024 and 0.25-mm section thickness. This allows us to acquire the image with twice the spatial resolution for both the in-plane and section directions. However, a halved image pixel size in both in-plane and section directions will increase the image noise by approximately a factor of 4 in photon detection statistics [23]. It requires the radiation dose to be increased by a factor of 16 to maintain the noise at the same level as the original pixel size. Reduction of the so-called “dose penalty” is achieved by applying the noise reduction reconstruction methods [24]. The most common method is iterative reconstruction algorithms that was said MBIR algorithms. This algorithm, compared with FBP, decreases noise, and maintains image quality with re-

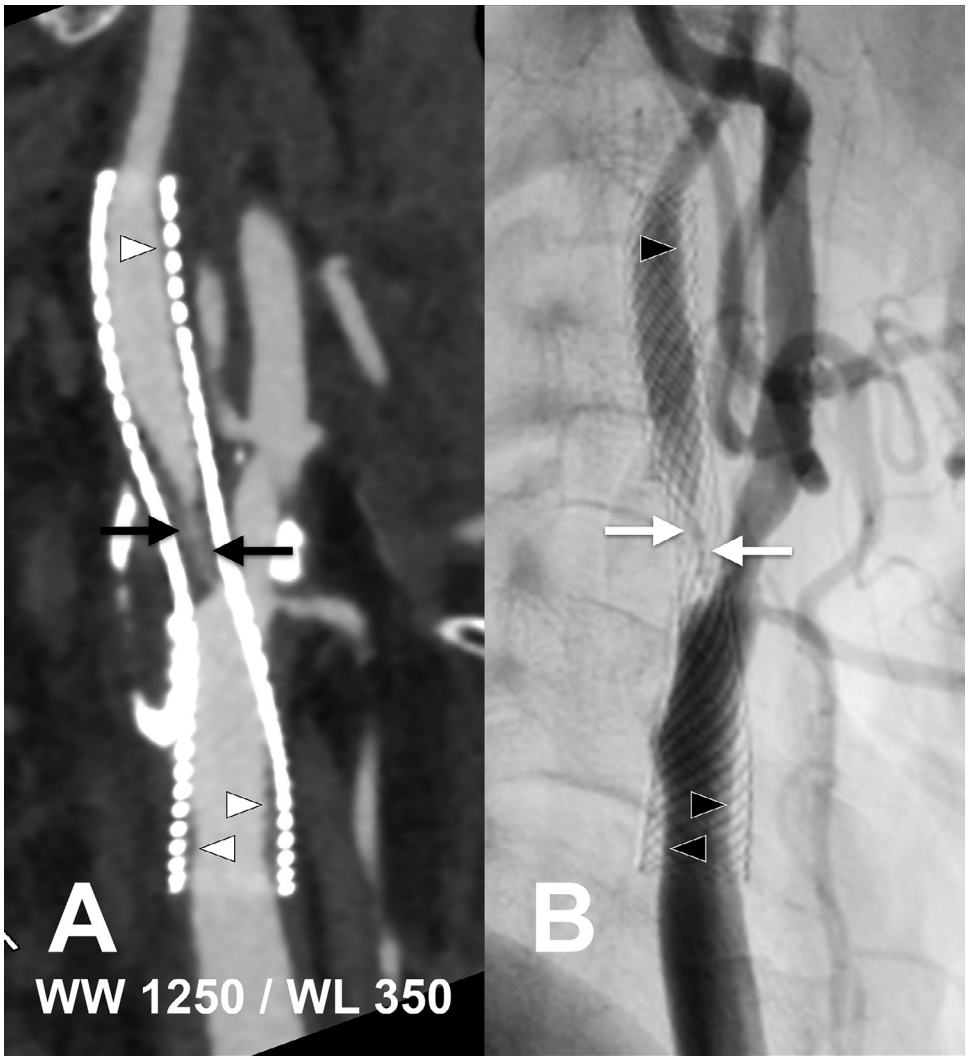

Fig. 2 – A 77-year-old-man. (A) Curved planar reformation image using MBIR reconstruction method indicated in-stent restenosis (black arrows) and intimal formation (white arrowheads). (B) Digital subtraction angiography revealed in-stent restenosis (white arrows) and intimal formation (black arrowheads).

duced doses [25,26]. Morisaka *et al.* reported that combining the UHRCT scanner system with MBIR resulted in further improvement of the vessel detectability and image noise reduction compared with the UHRCT with FBP [27]. Moreover, Yokomachi *et al.* reported that the MBIR algorithm improves diagnostic performance in the detection of neointimal formations after CAS [20].

Regarding radiation exposure, reported mean $CTDI_{vol}$ and DLP for carotid CTA using conventional CT scanners were 9.5 ± 0.6 mGy and 292.8 ± 46.2 mGy • cm, respectively [28]. Our results using a UHRCT scanner system were almost comparable (9.6 mGy and 341.8 ± 14.6 mGy • cm, respectively).

Orbach *et al.* reported that extremely wide window settings resulted in artificial widening of the measured lumen; these settings allow for the visualization of the struts of the stent and the cortices of bone structures (ie, at a window width of 1500 HU and window level of 1500 HU) [29]. However, these extremely wide window settings would prevent the evaluation of in-stent neointimal formations. We adjusted window settings that provided evaluation of native vessel segments (ie, at a window width of 1250 HU and window level of 350 HU). The combination of the UHRCT scanner system and MBIR allowed for appropriate window settings to visualize both soft tissue and metal structure without significant blooming artifacts.

In conclusion, the combination of the UHRCT scanner system with MBIR provided the detailed morphology of the carotid artery treated with CWS with reduced blooming artifacts. It may play a significant role in evaluating in-stent restenosis and vessel patency in follow-up examination of patients treated with carotid artery stenting.

Patient consent

This study protocol was approved by the Institutional Review Board in Tohoku University hospital (2020-1-413). Since this was a retrospective and noninvasive study, the requirement

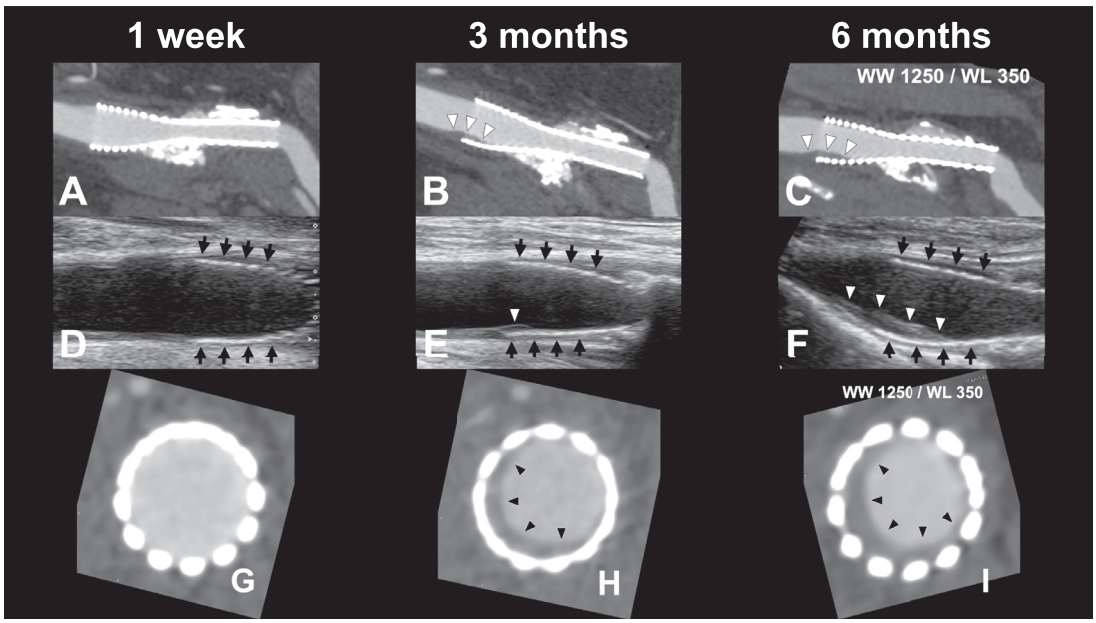

Fig. 3 – A 79-year-old-man. (A, B, and C) Curved planar reformation images. The changes in intimal formations over time are clearly shown (white arrowheads). (D, E, and F) Ultrasonography images. Black arrows indicate CWS, white arrowheads indicate time-dependent intimal formations. (G, H, and I) Cross-sectional images show the development of intimal formations over time (black arrowheads).

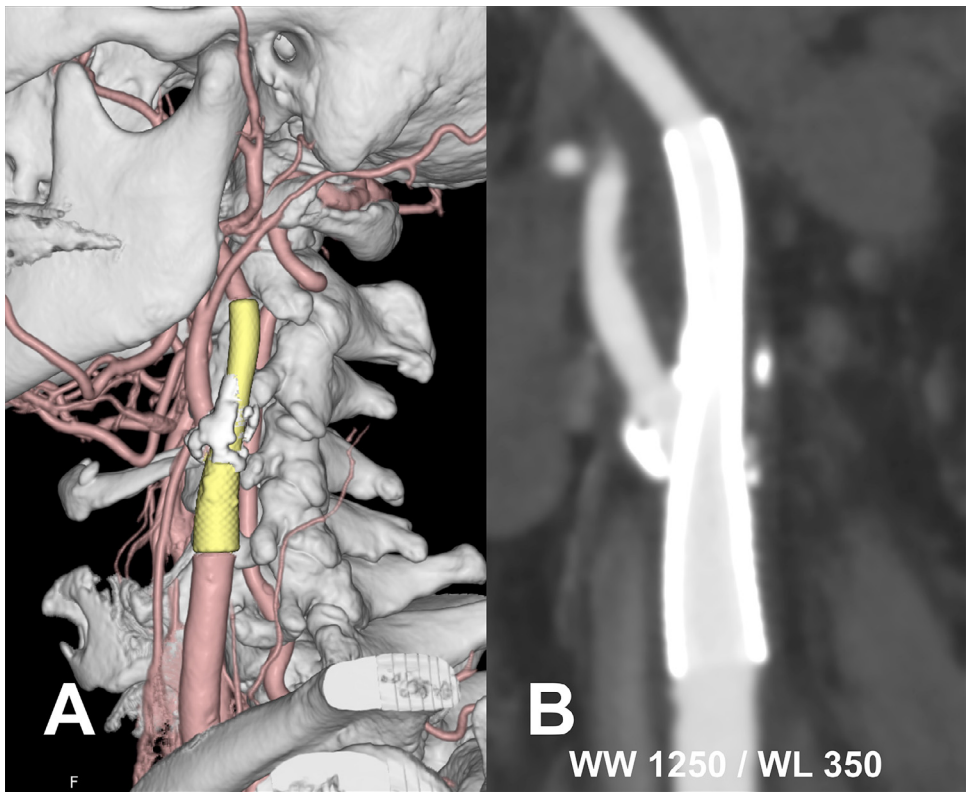

Fig. 4 – A 77-year-old-man. Computed tomography (CT) angiography of this case was performed using a conventional CT scanner. (A) Volume rendering image. (B) Cross-sectional image.

for written informed consent from patients was waived. A public notice that provided information on this study was instead given on the hospital's website.

Ethics approval

This study was received and approved by the Ethical Review Board of Tohoku University Hospital (2020-1-413).

REFERENCES

[1] Clark DJ, Lessio S, O'Donoghue M, Schainfeld R, Rosenfield K. Safety and utility of intravascular ultrasound-guided carotid artery stenting. Catheter Cardiovasc Interv 2004;63:355–62. doi:10.1002/ccd.20188.

[2] Wholey MH, Wholey M, Bergeron P, Diethrich EB, Henry M, Laborde JC, et al. Current global status of carotid artery stent placement. Cathet Cardiovasc Diagn 1998;44:1–6. doi:10.1002/(sici)1097-0304(199805)44:1⟨1::aid-ccd1⟩3.0.co;2-b.

[3] Yadav JS, Roubin GS, Iyer S, Vitek J, King P, Jordan WD, et al. Elective stenting of the extracranial carotid arteries. Circulation 1997;95:376–81. doi:10.1161/01.cir.95.2.376.

[4] Yadav JS, Wholey MH, Kuntz RE, Fayad P, Katzen BT, Mishkel GJ, et al. Protected carotid-artery stenting versus endarterectomy in high-risk patients. N Engl J Med 2004;351:1493–501. doi:10.1056/nejmoa040127.

[5] Gröschel K, Riecker A, Schulz JB, Ernemann U, Kastrup A. Systematic review of early recurrent stenosis after carotid angioplasty and stenting. Stroke 2005;36:367–73. doi:10.1161/01.str.0000152357.82843.9f.

[6] Lal BK, Beach KW, Roubin GS, Lutsep HL, Moore WS, Malas MB, et al. Restenosis after carotid artery stenting and endarterectomy: a secondary analysis of CREST, a randomised controlled trial. Lancet Neurol 2012;11:755–63. doi:10.1016/s1474-4422(12)70159-x.

[7] Bonati LH, Dobson J, Featherstone RL, Ederle J, Worp HBvan der, Borst GJde, et al. Long-term outcomes after stenting versus endarterectomy for treatment of symptomatic carotid stenosis: the International Carotid Stenting Study (ICSS) randomised trial. Lancet 2015;385:529–38. doi:10.1016/s0140-6736(14)61184-3.

[8] Watarai H, Kaku Y, Yamada M, Kokuzawa J, Tanaka T, Andoh T, et al. Follow-up study on in-stent thrombosis after carotid stenting using multidetector CT angiography. Neuroradiology 2009;51:243–51. doi:10.1007/s00234-009-0498-7.

[9] Nolz R, Wibmer A, Beitzke D, Gentzsch S, Willfort-Ehringer A, Lammer J, et al. Carotid artery stenting and follow-up: value of 64-MSCT angiography as complementary imaging method to color-coded duplex sonography. Eur J Radiol 2012;81:89–94. doi:10.1016/j.ejrad.2010.12.007.

[10] Kim CH, Kang J, Ryu W-S, Sohn C-H, Yoon B-W. Effects of carotid calcification on restenosis after carotid artery stenting: a follow-up study with computed tomography angiography. World Neurosurg 2018;117:e514–21. doi:10.1016/j.wneu.2018.06.068.

[11] Cademartiri F, Mollet N, Nieman K, Krestin GP, Feyter PJ de. Images in cardiovascular medicine. Neointimal hyperplasia in carotid stent detected with multislice computed tomography. Circulation 2003;108:e147. doi:10.1161/01.cir.0000103947.77551.9f.

[12] Lettau M, Kotter E, Bendszus M, Hähnel S. Carotid artery stents on CT angiography: in vitro comparison of different stent designs and sizes using 16-, 64- and 320-row CT scanners. J Neuroradiol 2014;41:259–68. doi:10.1016/j.neurad.2013.10.003.

[13] Sakai C, Sakai N, Okada T, Kuroiwa T, Ishihara H, Morizane A, et al. Computed tomography angiography of carotid stent. Interv Neuroradiol 2006;12:189–92. doi:10.1177/15910199060120s133.

[14] Lettau M, Sauer A, Heiland S, Rohde S, Bendszus M, Hähnel S. Carotid artery stents: in vitro comparison of different stent designs and sizes using CT angiography and contrast-enhanced MR angiography at 1.5T and 3T. AJNR Am J Neuroradiol 2009;30:1993–7. doi:10.3174/ajnr.a1743.

[15] Lettau M, Sauer A, Heiland S, Rohde S, Reinhardt J, Bendszus M, et al. In vitro comparison of different carotid artery stents: a pixel-by-pixel analysis using CT angiography and contrast-enhanced MR angiography at 1.5 and 3 T. Neuroradiology 2010;52:823–30. doi:10.1007/s00234-009-0625-5.

[16] Onishi H, Hori M, Ota T, Nakamoto A, Osuga K, Tatsumi M, et al. Phantom study of in-stent restenosis at high-spatial-resolution CT. Radiology 2018;289:255–60. doi:10.1148/radiol.2018180188.

[17] Yanagawa M, Hata A, Honda O, Kikuchi N, Miyata T, Uranishi A, et al. Subjective and objective comparisons of image quality between ultra-high-resolution CT and conventional area detector CT in phantoms and cadaveric human lungs. Eur Radiol 2018;28:5060–8. doi:10.1007/s00330-018-5491-2.

[18] Li K, Garrett J, Ge Y, Chen G-H, Chen G-H. Statistical model based iterative reconstruction (MBIR) in clinical CT systems. Part II. Experimental assessment of spatial resolution performance. Med Phys 2014;41:071911. doi:10.1118/1.4884038.

[19] Li K, Tang J, Chen G-H. Statistical model based iterative reconstruction (MBIR) in clinical CT systems: experimental assessment of noise performance. Med Phys 2014;41:041906. doi:10.1118/1.4867863.

[20] Yokomachi K, Tatsugami F, Higaki T, Kume S, Sakamoto S, Okazaki T, et al. Neointimal formation after carotid artery stenting: phantom and clinical evaluation of model-based iterative reconstruction (MBIR). Eur Radiol 2019;29:161–7. doi:10.1007/s00330-018-5598-5.

[21] Package insert of the Carotid WALLSTENT Monorail Endoprosthesis. Food and Drug Administration (US). Available at: www.accessdata.fda.gov/cdrh_docs/pdf5/P050019c.pdf (accessed June 2, 2008).

[22] Köhler M, Burg MC, Bunck AC, Heindel W, Seifarth H, Maintz D. Dual-source CT angiography of peripheral arterial stents: in vitro evaluation of 22 different stent types. Radiol Res Pract 2011:103873 2011. doi:10.1155/2011/103873.

[23] Chesler DA, Riederer SJ, Pelc NJ. Noise due to photon counting statistics in computed X-ray tomography. J Comput Assist Tomogr 1977;1:64–74. doi:10.1097/00004728-197701000-00009.

[24] Wang J, Fleischmann D. Improving spatial resolution at CT: development, benefits, and pitfalls. Radiology 2018;289:261–2. doi:10.1148/radiol.2018181156.

[25] Higaki T, Nakamura Y, Fukumoto W, Honda Y, Tatsugami F, Awai K. Clinical application of radiation dose reduction at abdominal CT. Eur J Radiol 2019;111:68–75. doi:10.1016/j.ejrad.2018.12.018.

[26] Greffier J, Frandon J, Larbi A, Beregi JP, Pereira F. CT iterative reconstruction algorithms: a task-based image quality assessment. Eur Radiol 2020;30:487–500. doi:10.1007/s00330-019-06359-6.

[27] Morisaka H, Shimizu Y, Adachi T, Fukushima K, Arai T, Yamamura W, et al. Effect of ultra high-resolution computed tomography and model-based iterative reconstruction on detectability of simulated submillimeter artery. J Comput Assist Tomo 2020;44:32–6. doi:10.1097/rct.0000000000000963.
[28] Eller A, Wuest W, Kramer M, May M, Schmid A, Uder M, et al. Carotid CTA: radiation exposure and image quality with the use of attenuation-based, automated kilovolt selection. Am J Neuroradiol 2014;35:237–41. doi:10.3174/ajnr.a3659.
[29] Orbach DB, Pramanik BK, Lee J, Maldonado TS, Riles T, Grossman RI. Carotid artery stent implantation: evaluation with multi-detector row CT angiography and virtual angioscopy–initial experience. Radiology 2006;238:309–20. doi:10.1148/radiol.2381042106.